Mineralogical Magazine (2019), **83**, 153–160
doi:10.1180/mgm.2018.117

CAMBRIDGE UNIVERSITY PRESS

Feynmanite, a new sodium uranyl sulfate mineral from Red Canyon, San Juan County, Utah, USA

Anthony R. Kampf[1], Travis A. Olds[2,§], Jakub Plášil[3], Joe Marty[4] and Samuel N. Perry[2]

[1]Mineral Sciences Department, Natural History Museum of Los Angeles County, 900 Exposition Boulevard, Los Angeles, CA 90007, USA; [2]Department of Civil and Environmental Engineering and Earth Sciences, University of Notre Dame, Notre Dame, IN 46556, USA; [3]Institute of Physics ASCR, v.v.i., Na Slovance 1999/2, 18221 Prague 8, Czech Republic and [4]5199 East Silver Oak Road, Salt Lake City, UT 84108, USA

Abstract

The new mineral feynmanite, $Na(UO_2)(SO_4)(OH)\cdot 3.5H_2O$, was found in both the Blue Lizard and Markey mines, San Juan County, Utah, USA, where it occurs as a secondary phase on pyrite-rich asphaltum in association with chinleite-(Y), gypsum, goethite, natrojarosite, natrozippeite, plášilite, shumwayite (Blue Lizard) and wetherillite (Markey). The mineral is pale greenish yellow with a white streak and fluoresces bright greenish white under a 405 nm laser. Crystals are transparent with a vitreous lustre. It is brittle, with a Mohs hardness of ~2, irregular fracture and one perfect cleavage on {010}. The calculated density is 3.324 g cm^{-3}. Crystals are thin needles or blades, flattened on {010} and elongate on [100], exhibiting the forms {010}, {001}, {101} and {10$\bar{1}$}, and are up to ~0.1 mm in length. Feynmanite is optically biaxial (–), with $\alpha = 1.534(2)$, $\beta = 1.561(2)$ and $\gamma = 1.571(2)$ (white light); $2V_{meas.} = 62(2)°$; no dispersion; and optical orientation: X = **b**, $Y \approx$ **a**, $Z \approx$ **c**. It is weakly pleochroic: X = colourless, Y = very pale green yellow and Z = pale green yellow ($X < Y < Z$). Electron microprobe analyses (WDS mode) provided $(Na_{0.84}Fe_{0.01})(U_{1.01}O_2)(S_{1.01}O_4)(OH)\cdot 3.5H_2O$. The five strongest powder X-ray diffraction lines are [d_{obs} Å(I)(hkl)]: 8.37(100)(010), 6.37(33)($\bar{1}$01,101), 5.07(27)($\bar{1}$11,111), 4.053(46)(004,021) and 3.578(34)(120). Feynmanite is monoclinic, has space group $P2/n$, $a = 6.927(3)$, $b = 8.355(4)$, $c = 16.210(7)$ Å, $\beta = 90.543(4)°$, $V = 938.1(7)$ Å^3 and $Z = 4$. The structure of feynmanite ($R_1 = 0.0371$ for 1879 $I_o > 2\sigma I$) contains edge-sharing pairs of pentagonal bipyramids that are linked by sharing corners with SO_4 groups, yielding a $[(UO_2)_2(SO_4)_2(OH)_2]^{2-}$ sheet based on the phosphuranylite anion topology. The sheet is topologically identical to those in deliensite, johannite and plášilite. The dehydration of feynmanite to plášilite results in interlayer collapse involving geometric reconfiguration of the sheets and the ordering of Na.

Keywords: feynmanite, new mineral, uranyl sulfate, crystal structure, phosphuranylite anion topology, Markey mine, Blue Lizard mine, Red Canyon, Utah, USA

(Received 6 November 2017; accepted 16 February 2018)

Introduction

Prior to the discovery of a wide variety of new Na uranyl sulfate minerals at the Blue Lizard mine in Red Canyon, Utah, USA, only one Na uranyl sulfate, natrozippeite, was known to occur in Nature. Since 2013 a further 11 new Na uranyl sulfates have been described from the Blue Lizard mine (Kampf *et al.*, 2017*b*). To these, we now add the Na uranyl sulfate, feynmanite, which has also been found at the nearby Markey mine.

These minerals crystallise as uranium- and sulfate-containing groundwater evaporates on the mine walls, often in close proximity to uranium ore replacements of organic material (wood and other plant remains), the source of the uranium. The Na uranyl sulfates of Red Canyon are notable for their range in U–S–Na contents and for their topological variety, displaying topologies based on isolated clusters (e.g. klaprothite; Kampf *et al.*, 2017*b*), chains (e.g. fermiite; Kampf *et al.*, 2015*a*) and sheets (e.g. plášilite; Kampf *et al.*, 2015*b*). Their formation is interesting and complex, and distinct arrangements are observed, even for minerals with nominally identical U–S–Na contents (although generally different amounts of OH and/or H_2O). Our studies of the unique topological arrangements of Na uranyl sulfates continues, as numerous additional new minerals from Red Canyon await final characterization.

Feynmanite (/'fain mən ait/) is named for American physicist Richard Feynman (1918–1988), one of the most important physicists of the 20th Century. Although well-known for his contributions to the Manhattan Project (hence the connection to uranium), it was his work on quantum electrodynamics that earned him the Nobel Prize in Physics in 1965.

The new mineral and name were approved by the International Mineralogical Association Commission on New Minerals, Nomenclature and Classification (IMA2017-035, Kampf, 2017*a*). The description is based on four cotype specimens deposited in the collections of the Natural History Museum of Los Angeles County, 900 Exposition Boulevard, Los Angeles, CA 90007, USA, catalogue numbers 66590 and 66591 (Blue Lizard mine) and 66592 and 66593 (Markey mine).

Occurrence

Feynmanite was found underground in both the Blue Lizard mine (37°33′26″N, 110°17′44″W) and the Markey mine (37°32′57″N, 110°18′08″W), Red Canyon, White Canyon District, San Juan County, Utah, USA. The Markey mine is located ~1 km southwest of the Blue Lizard mine. The Blue Lizard mine is on the west-facing side of Red Canyon and the Markey mine is on the

Author for correspondence: Anthony R. Kampf, Email: akampf@nhm.org
§Current address: School of Mechanical and Materials Engineering, Washington State University, Pullman, WA 99164, USA
Associate Editor: Mark Welch
Cite this article: Kampf A.R., Olds T.A., Plášil J., Marty J. and Perry S.N. (2019) Feynmanite, a new sodium uranyl sulfate mineral from Red Canyon, San Juan County, Utah, USA. *Mineralogical Magazine* **83**, 153–160. https://doi.org/10.1180/mgm.2018.117

east-facing side. Both are ~72 km west of the town of Blanding, Utah, and ~22 km southeast of Good Hope Bay on Lake Powell. The geology of the Blue Lizard and Markey mines is quite similar (Chenoweth, 1993; Kampf, *et al.*, 2015*a*), although the mineralogy of the Markey mine is notably richer in carbonate phases. The following information on the mines and their geology is taken largely from Chenoweth (1993).

The deposit exploited by the Blue Lizard mine was first recognised in the summer of 1898 by John Wetherill while leading an archaeological expedition into Red Canyon. He noted yellow stains around a petrified tree. At that spot, he built a rock monument, in which he placed a piece of paper to claim the minerals. Although he never officially recorded his claim, 45 years later, in 1943, he described the spot to Preston V. Redd of Blanding, Utah, who went to the site, found Wetherill's monument and claimed the area as the Blue Lizzard claim (note alternate spelling). Underground workings to mine uranium were not developed until 1951, the highest production occurred in the late 1950s and the mine last produced ore in 1970.

The Markey group of claims, was staked in 1949 by Jim Rigg of Grand Junction, Colorado, and was purchased from Rigg and others by the Anaconda Copper Mining Company on June 1, 1951. After limited exploration and production, the mine closed in 1955. The mine was subsequently acquired from Anaconda by Calvin Black of Blanding, Utah, under whose ownership the mine operated from 1960 to 1982 and was a leading producer in the district for nearly that entire period.

The uranium deposits in Red Canyon occur within the Shinarump member of the Upper Triassic Chinle Formation, in channels incised into the reddish-brown siltstones of the underlying Lower Triassic Moenkopi Formation. The Shinarump member consists of medium- to coarse-grained sandstone, conglomeratic sandstone beds and thick siltstone lenses. Accumulations of wood and other plant material in the channels provided reducing environments that caused the deposition of the ore minerals, which are found as replacements of the organic material (typically manifesting as asphaltum) and as disseminations in the enclosing sandstone. Since the mines closed, oxidation of primary ores in the humid underground environment has produced a variety of secondary minerals as efflorescent crusts on the surfaces of mine walls.

Feynmanite is a rare mineral in the secondary mineral assemblages at both mines, where it occurs on pyrite-rich asphaltum matrix. At the Blue Lizard mine, it occurs with chinleite-(Y), gypsum, goethite, natrojarosite, natrozippeite, plášilite and shumwayite. At the Markey mine, it occurs with chinleite-(Y), gypsum, natrojarosite, natrozippeite, plášilite and wetherillite. Feynmanite crystals are very prone to dehydration, generally yielding fine-grained plášilite; well-formed plášilite crystals are not found in association with feynmanite. Numerous other secondary minerals have been found at both mines (cf. Kampf *et al.*, 2017*b* and Kampf *et al.*, 2018).

Considering that feynmanite has thus far been found only on asphaltum at both the Blue Lizard and Markey mines, the possible role of the asphaltum in the formation/stability of feynmanite is worth commenting on. The asphaltum certainly provides a reducing environment; however, this does not seem to be a factor. Similarly, high U content, often present in the asphaltum, does not in itself explain why feynmanite is found on asphaltum rather than quartz-rich matrix because phases with similar Na:U:S ratios (e.g. plášilite) are found on quartz matrix. It seems that the most likely factor is the capacity of the asphaltum to retain moisture and, thereby, provide a more hospitable and stable substrate for the feynmanite crystals.

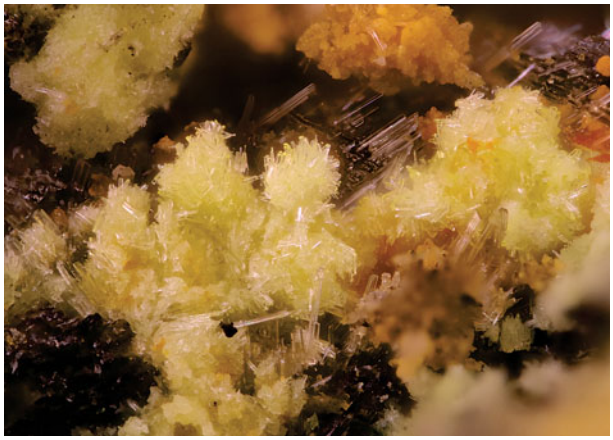

Fig. 1. Clusters of greenish-yellow feynmanite blades with colourless gypsum and dull orange natrojarosite on asphaltum from the Markey mine; the horizontal field of view is 2 mm; Natural History Museum of Los Angeles County, catalogue number 66593.

Physical and optical properties

Feynmanite crystals are thin needles or blades, up to ~0.1 mm long, growing in random 'jackstraw' aggregates (Fig. 1). Blades are flattened on {010} and elongate on [100]; they exhibit the forms {010}, {001}, {101} and {10$\bar{1}$} (Fig. 2). No twinning was observed.

The mineral is pale greenish yellow with a white streak and fluoresces bright greenish white under a 405 nm laser. Crystals are transparent and have vitreous lustre. The tenacity is brittle, the Mohs hardness is ~2, the fracture is irregular and there is one perfect cleavage parallel to {010}. The density could not be measured because the tiny crystals are too difficult to see in

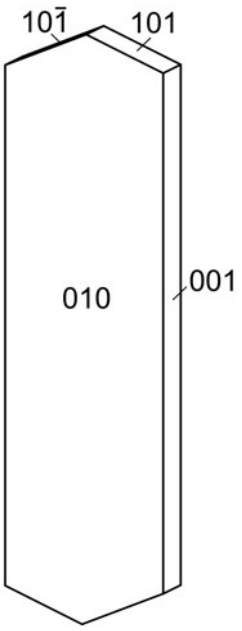

Fig. 2. Crystal drawing of feynmanite with clinographic projection in nonstandard orientation and [100] vertical.

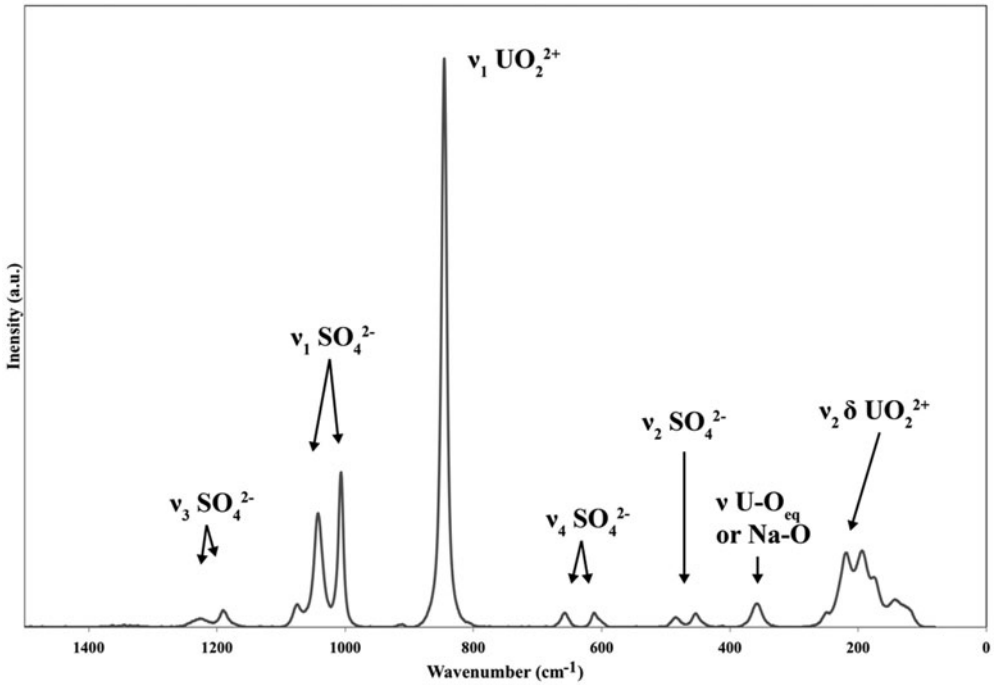

Fig. 3. The Raman spectrum of feynmanite recorded with a 785 nm laser.

density liquids, such as methylene iodide. The calculated density is 3.324 g cm^{-3} for the empirical formula and 3.321 g cm^{-3} for the ideal formula. At room temperature, the mineral dissolves very slowly in H_2O (minutes) and dissolves immediately in dilute HCl.

Optically, feynmanite is biaxial (–), with $\alpha = 1.534(2)$, $\beta = 1.561(2)$ and $\gamma = 1.571(2)$ (measured in white light). The 2V measured directly on a spindle-stage is 62(2)°; the calculated 2V is 61.7°. Dispersion is imperceptible. The mineral is weakly pleochroic: X = colourless, Y = very pale green yellow, Z = pale green yellow; and $X < Y < Z$. The optical orientation is $X = \mathbf{b}$, $Y \approx \mathbf{a}$ and $Z \approx \mathbf{c}$.

Raman spectroscopy

The Raman spectrum of feynmanite from the Markey mine was recorded using a Bruker Instruments Sentinel-785 laser head

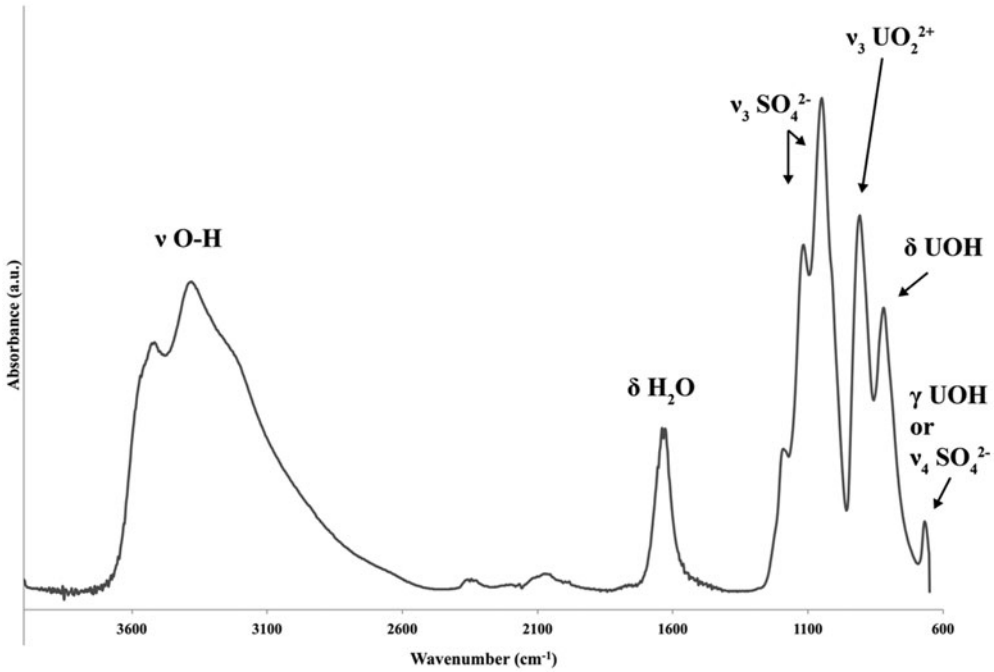

Fig. 4. The infrared spectrum (ATR) of feynmanite.

mounted on a Nikon Optiphot-2 microscope with Peltier-cooled CCD detector and integrated 785 nm diode laser, operated at 200 mW, with a spot size of 100 μm and ~5 cm^{-1} resolution (Fig. 3). The spectrum was acquired using a 10× objective, from 1500 to 80 cm^{-1} using five 3 s exposures, with five repeated acquisitions to improve the signal-to-noise ratio. The spectrometer was calibrated with Bruker software-controlled procedures (*Opus* software) using neon emission lines (wavelength calibration), and Tylenol® bands (frequency calibration). A background correction was applied using the *Opus* software.

The split triply degenerate $\nu_3(SO_4)^{2-}$ antisymmetric stretching vibrations occur as weak bands at 1219 and 1189 cm^{-1}, and several medium-strong bands at 1075, 1042 and 1006 cm^{-1} are assignable to the $\nu_1(SO_4)^{2-}$ symmetric stretching vibrations. The $\nu_1(UO_2)^{2+}$ symmetric stretching vibration is present as a very strong band at 846 cm^{-1}. A very weak band at 911 cm^{-1} is assigned to the $\nu_3(UO_2)^{2+}$ antisymmetric stretch. Bartlett and Cooney (1989) provide an empirical relationship to derive the approximate U–O_{yl} bond lengths from the band positions assigned to the $(UO_2)^{2+}$ stretching vibrations, which give 1.76 Å

Table 1. Chemical composition for feynmanite.

Constituent	Mean	Range	S.D.	Standard
Na_2O	5.56	5.13–6.43	0.75	Albite
FeO	0.13	0.01–0.25	0.12	Hematite
UO_3	61.77	58.75–64.05	2.73	Synthetic UO_2
SO_3	17.19	16.82–17.88	0.59	Celestine
H_2O*	15.35			
Total	100.00			

* based on the structure; S.D. – standard deviation.

Table 2. Powder X-ray data (*d* in Å) for feynmanite. Only calculated lines with $I \geq 2$ are listed.

I_{obs}	I_{calc}	d_{obs}	d_{calc}	*hkl*
100	100	8.37	8.3550	010
18	19	7.42	7.4265	011
33	19, 23	6.37	6.3914, 6.3478	$\bar{1}01$, 101
20	22	5.33	5.3325	110
27	14, 15	5.07	5.0764, 5.0545	$\bar{1}11$, 111
4	7	4.538	4.5370	013
7	7, 4	4.260	4.2800, 4.2408	$\bar{1}03$, 103
9	12	4.180	4.1775	020
46	30, 27	4.053	4.0523, 4.0453	004, 021
	2		3.8093	$\bar{1}13$
	2		3.7816	113
25	25	3.649	3.6461	014
28	34	3.578	3.5773	120
25	30	3.467	3.4633	200
6	7	3.292	3.3049	023
25	7, 4, 19	3.213	3.2378, 3.2151, 3.1994	$\bar{1}14$, 114, 210
6	2, 4	3.150	3.1440, 3.1336	$\bar{2}11$, 211
	3		3.0223	015
20	8, 15	2.934	2.9469, 2.9256	$\bar{1}05$, 105
	4		2.9087	024
15	8, 4, 4	2.768	2.7791, 2.7612, 2.7448	$\bar{1}15$, 115, 031
17	6, 8, 3	2.675	2.6884, 2.6753, 2.6662	$\bar{1}24$, 124, 220
18	11, 2, 10, 9	2.625	2.6452, 2.6340, 2.6206, 2.5840	$\bar{2}04$, $\bar{2}21$, 204, 130
11	3	2.566	2.5611	025
20	9, 10, 3	2.507	2.5218, 2.5005, 2.4755	$\bar{2}14$, 214, 033
4	3	2.405	2.3979	$\bar{2}23$
	2		2.3841	223
6	2, 2, 2	2.284	2.2889, 2.2872, 2.2828	$\bar{3}01$, $\bar{2}15$, 301
	2		2.2673	215
6	2	2.231	2.2349	$\bar{2}24$
6	3, 2, 4	2.212	2.2255, 2.2199, 2.2021	310, 224, 311
10	5, 4	2.184	2.1822, 2.1752	$\bar{1}34$, 134
8	3, 3	2.153	2.1508, 2.1495	126, 231
10	6, 2, 2	2.123	2.1305, 2.1159, 2.1125	$\bar{3}03$, 303, 035
6	4	2.087	2.0888	040
10	3, 4, 6	2.061	2.0716, 2.0667, 2.0519	041, $\bar{2}25$, 225
15	8, 8	2.026	2.0262, 2.0208	008, 320
7	2, 5	2.005	2.0098, 1.9998	233, 140
6	2, 2, 2	1.9770	1.9854, 1.9841, 1.9691	$\bar{1}41$, 141, 018
5	2	1.9495	1.9432	314
9	2, 4	1.8861	1.8986, 1.8891	$\bar{1}18$, $\bar{3}05$
5	2, 2, 3, 2	1.8618	1.8771, 1.8738, 1.8723, 1.8566	$\bar{1}43$, 143, 305, 044
	2		1.8426	$\bar{3}15$
8	2, 5	1.8201	1.8270, 1.8144	315, $\bar{3}24$
15	2, 4, 2, 2, 2, 2	1.7975	1.8085, 1.8024, 1.7986, 1.7953, 1.7914, 1.7886	$\bar{2}35$, 324, 235, $\bar{1}44$, 144, 240
	2		1.7805	037
15	5, 3, 3, 4	1.769	1.7775, 1.7667, 1.7593, 1.7561	330, $\bar{1}28$, 128, $\bar{2}08$
14	3, 3, 3, 4	1.7441	1.7471, 1.7417, 1.7391, 1.7317	$\bar{1}09$, 208, 109, 400
12	2, 3, 2, 3	1.7123	1.7186, 1.7101, 1.7050, 1.7026	$\bar{2}18$, $\bar{1}19$, 218, 119
9	3, 4	1.6938	1.6999, 1.6956	145, 410

Table 3. Data collection and structure refinement details for feynmanite.*

Crystal data	
Structural formula	$Na_{0.97}(UO_2)(SO_4)(OH)\cdot 3.5H_2O$
Crystal size (μm)	68 × 61 × 5
Crystal system, space group	monoclinic, *P*2/*n*
Temperature	298(2) K
a, *b*, *c* (Å)	6.927(3), 8.355(4), 16.210(7)
β (°)	90.543(4)
V (Å^3)	938.1(7)
Z	4
Density (for above formula, g/cm^3)	3.316
Data collection	
Diffractometer	Bruker Apex II Quazar
X-ray radiation/power	MoKα (λ = 0.71075 Å)/50 kV, 40 mA
Absorption correction	Multi-scan semi-empirical using equivalent reflections in *SADABS-2012*
Absorption coefficient (mm^{-1})	17.606
F(000)	843
θ range (°)	2.44 to 29.03
Reflections collected/unique	10,605/2358; R_{int} = 0.052
Reflections with $I > 2\sigma I$	1879
Completeness to θ = 29.03°	94.1%
Index ranges	$-8 \le h \le 9$, $-11 \le k \le 11$, $-21 \le l \le 21$
Refinement	
Refinement method	Full-matrix least-squares on F^2
Restraints/parameters	0/150
GoF	1.007
Final *R* indices [$F > 4\sigma(F)$]	R_1 = 0.0371, wR_2 = 0.0817
R indices (all data)	R_1 = 0.0537, wR_2 = 0.0886
Largest diff. peak/hole (*e*$^-$ Å^{-3})	+3.76/−2.50

*$R_{int} = \Sigma|F_o^2 - F_o^2(\text{mean})|/\Sigma[F_o^2]$. GoF = $S = \{\Sigma[w(F_o^2 - F_c^2)^2]/(n-p)\}^{1/2}$. $R_1 = \Sigma||F_o| - |F_c||/\Sigma|F_o|$. $wR_2 = \{\Sigma[w(F_o^2 - F_c^2)^2]/\Sigma[w(F_o^2)^2]\}^{1/2}$; $w = 1/[\sigma^2(F_o^2) + (aP)^2 + bP]$ where *a* is 0.0537, *b* is 0 and *P* is $[2F_c^2 + \text{Max}(F_o^2, 0)]/3$.

(ν_1) and 1.77 Å (ν_3), in accordance with U–O_{yl} bond lengths from the X-ray data (1.75 Å and 1.76 Å).

Weak bands found at 658 and 612 cm^{-1} are attributed to the split, triply degenerate $\nu_4(\delta)(SO_4)^{2-}$ bending vibrations, and those at 484 and 454 cm^{-1} to the split doubly degenerate $\nu_2(\delta)(SO_4)^{2-}$ bending vibrations. A weak band at 358 cm^{-1} is either due to ν (U–$O_{equatorial}$) stretching vibrations or Na–O stretches (e.g. Volkovich *et al.*, 1998; Plášil *et al.*, 2010; Kampf *et al.*, 2015*a*,*b*). Bands at 249, 219, 194 and 176 cm^{-1} arise from $\nu_2(\delta)$ U–O–U bending modes. Remaining bands <150 cm^{-1} are assigned to external lattice vibration modes.

Infrared spectroscopy

An attenuated total reflectance (ATR) Fourier transform infrared (FTIR) spectrum of feynmanite from the Markey mine was obtained using a SENSIR Technologies IlluminatIR with a liquid N_2 cooled MCT detector mounted to an Olympus BX51 microscope. An ATR objective (ZnSe/diamond) was pressed into crystals of feynmanite and the spectrum was measured from 4000 to 650 cm^{-1} (Fig. 4).

Stretching vibrations ν(OH) occur between 2800 and 3600 cm^{-1}, with maxima at 3381 and 3517 cm^{-1}, and a shoulder around 3220 cm^{-1}. Approximate O–H···O hydrogen bond-lengths calculated from the observed stretching frequencies lie within the range ~2.9 to 2.6 Å using the correlation function given by Libowitzky (1999). Several broad, low intensity bands between 2345–2070 cm^{-1} correspond to combination bands (δ H_2O and L H_2O). Medium-strong bands found at 1639 and 1628 cm^{-1} are assigned as the ν_2-(δ)-bending vibrations of structurally unique H_2O groups.

Absorption bands at 1190, 1116 and 1048 cm^{-1} are assigned to the split triply degenerate $\nu_3(SO_4)^{2-}$ antisymmetric stretching vibration. A shouldering band centred at 1011 cm^{-1} is probably attributed to the IR-active $\nu_1(SO_4)^{2-}$ symmetric stretch.

The strong antisymmetric stretch $\nu_3(UO_2)^{2+}$ occurs at 909 cm^{-1}. No evidence is found for the presence of the symmetric $\nu_1(UO_2)^{2+}$ stretch. The uranyl cation bond length inferred from the IR spectrum of feynmanite using the empirical relation given by Bartlett and Cooney (1989) is 1.77 Å, and agrees well with the structure.

A strong band at 818 cm^{-1} is assigned as the δ U–OH (out-of-plane bending) mode. The $\nu_4(SO_4)^{2-}$ mode may coincide with either γ U–OH (out-of-plane bending) or librations of H_2O groups for the weak band at 669 cm^{-1}. According to Čejka (1999) the presence of δ U–OH between 800–900 cm^{-1}, γ U–OH from 600–700 cm^{-1} and fine bands at ~3500 cm^{-1} are characteristic to OH groups bridging two uranyl cations.

Composition

Chemical analyses (3) were performed using a Cameca SX-50 electron microprobe (wavelength dispersive spectroscopy mode) operating at an accelerating voltage of 15 kV, with a beam current

Table 4. Atom coordinates and displacement parameters (Å^2) for feynmanite.

	x/*a*	*y*/*b*	*z*/*c*	U_{eq}	U^{11}	U^{22}	U^{33}	U^{23}	U^{13}	U^{12}
U	0.74439(4)	0.40606(4)	0.36948(2)	0.01707(11)	0.01353(16)	0.02393(18)	0.01374(16)	−0.00056(12)	−0.00060(10)	0.00003(12)
S	0.2468(3)	0.5059(3)	0.41111(11)	0.0210(4)	0.0131(9)	0.0384(13)	0.0115(8)	−0.0005(8)	0.0001(7)	0.0003(8)
Na1*	0.7160(12)	−0.0931(9)	0.3631(5)	0.035(3)	0.036(5)	0.022(5)	0.047(6)	0.002(3)	0.001(4)	0.007(3)
Na2*	¼	0.8584(10)	¼	0.027(3)	0.017(4)	0.031(5)	0.033(5)	0	0.005(3)	0
Na3*	0.779(3)	−0.109(2)	0.6233(11)	0.036(9)	0.058(16)	0.023(12)	0.027(12)	−0.002(8)	0.008(10)	−0.009(9)
O1	0.2378(9)	0.5987(8)	0.3348(4)	0.0324(15)	0.036(4)	0.045(4)	0.016(3)	0.006(3)	0.000(2)	−0.002(3)
O2	0.2596(8)	0.6163(7)	0.4820(3)	0.0270(14)	0.024(3)	0.042(4)	0.015(3)	0.000(2)	0.002(2)	−0.007(3)
O3	0.4148(8)	0.3956(7)	0.4119(4)	0.0266(13)	0.016(3)	0.035(4)	0.029(3)	0.004(3)	0.003(2)	0.002(2)
O4	0.0725(8)	0.4033(7)	0.4196(3)	0.0269(13)	0.016(3)	0.042(4)	0.023(3)	0.000(3)	−0.002(2)	−0.001(2)
O5	0.7405(7)	0.6170(7)	0.3759(3)	0.0224(13)	0.020(3)	0.023(3)	0.024(3)	−0.001(2)	0.001(2)	0.000(2)
O6	0.7480(7)	0.1942(7)	0.3653(3)	0.0239(13)	0.021(3)	0.030(4)	0.020(3)	−0.002(2)	−0.001(2)	−0.001(3)
OH	0.5595(7)	0.4159(7)	0.2483(3)	0.0233(12)	0.014(2)	0.041(4)	0.015(2)	−0.002(2)	0.002(2)	0.003(2)
OW1	0.8389(18)	−0.0953(10)	0.4966(7)	0.083(3)	0.123(10)	0.048(6)	0.076(7)	−0.002(5)	−0.019(7)	−0.010(5)
OW2	¼	0.1657(16)	¼	0.084(5)	0.098(11)	0.050(8)	0.103(11)	0	−0.044(9)	0
OW3	0.422(2)	−0.0885(11)	0.3955(7)	0.096(4)	0.142(11)	0.050(6)	0.096(8)	−0.001(5)	−0.022(8)	−0.014(6)
OW4a*	0.921(6)	−0.109(2)	0.2828(11)	0.050(9)	0.04(2)	0.050(11)	0.059(11)	0.010(7)	0.013(9)	−0.013(9)
OW4b*	0.027(6)	0.888(3)	0.2917(18)	0.071(8)	0.017(16)	0.062(13)	0.14(2)	0.033(12)	0.013(12)	0.003(10)

*Occupancies: Na1: 0.48(2); Na2: 0.60(2); Na3: 0.19(2); and OW4a/b: 0.52/0.48(7).

Table 5. Selected bond distances (Å) for feynmanite.*

Na1–OW3	2.108(17)	Na2–OW4a ×2	2.36(4)	Na3–OW1	2.10(2)
Na1–OW1	2.319(13)	Na2–OW2	2.567(16)	Na3–OW2	2.120(19)
Na1–O6	2.411(9)	Na2–O1 ×2	2.570(9)	Na3–OW3	2.18(2)
Na1–O5	2.437(9)	Na2–OW3 ×2	2.670(12)	Na3–OW4b	2.66(4)
Na1–OW4b	2.46(4)	<Na2–O>	2.538	Na3–O4	2.76(2)
Na1–OW4a	2.54(3)			Na3–O3	2.804(19)
<Na1–O>	2.379			<Na3–O>	2.437
U–O5	1.766(6)	S–O1	1.461(6)		
U–O6	1.771(6)	S–O2	1.475(6)		
U–OH	2.337(5)	S–O3	1.484(6)		
U–OH	2.355(5)	S–O4	1.488(6)		
U–O3	2.392(6)	<S–O>	1.477		
U–O4	2.406(5)				
U–O2	2.416(5)				
<U–O_{Ur}>	1.769				
<U–O_{eq}>	2.381				

* Note that very short distances between Na sites and partially occupied OW4 sites are not included. Also, note the rather short Na1–OW3, Na2–OW1, Na2–OW2 and Na2–OW3 listed; this may be an artefact of the disorder in the interlayer region, considering that the OW1, OW2 and OW3 sites have high displacement parameters.

of 10 nA and 25 μm spot diameter. Feynmanite from the Markey mine contains appreciable U, S and Na, with minor Fe. No other elements were detected. Matrix effects were accounted for using the *PAP* correction routine (Pouchou and Pichoir, 1985). Volatilisation of Na was corrected for by zero-time correction. Due to the limited amount of material available, the H_2O content was not measured and is instead calculated by stoichiometry with respect to the structure. The empirical formula is calculated on the basis of 10.5 O atoms per formula unit (apfu). Analytical data are given in Table 1.

The empirical formula (calculated on the basis of 10.5 O apfu) is $(Na_{0.84}Fe_{0.01})(U_{1.01}O_2)(S_{1.01}O_4)(OH)\cdot 3.5H_2O$. The ideal formula is $Na(UO_2)(SO_4)(OH)\cdot 3.5H_2O$, which requires Na_2O 6.61, UO_3 60.97, SO_3 17.07, H_2O 15.36, total 100 wt.%. The Gladstone-Dale compatibility index $1 - (K_P/K_C)$ for the empirical formula is –0.003, in the superior range (Mandarino, 2007), using $k(UO_3) = 0.118$, as provided by Mandarino (1976).

X-ray crystallography and structure refinement

Powder X-ray diffraction studies were conducted on feynmanite from the Blue Lizard mine using a Rigaku R-Axis Rapid II curved imaging plate microdiffractometer, with monochromatised Mo*K*α radiation (λ = 0.71075 Å). A cluster of crystals was used to obtain the powder diffraction pattern, employing a Gandolfi-like motion on the ϕ and ω axes to randomise the sample. Observed *d* values and intensities were derived by profile fitting using *JADE 2010* software (Materials Data, Inc.). The powder data presented in Table 2 show good agreement with the pattern calculated from the structure determination. Unit-cell parameters refined from the powder data using *JADE 2010* with whole-pattern fitting are: $a = 6.934(3)$, $b = 8.367(3)$, $c = 16.239(3)$ Å, $\beta = 90.494(12)°$ and $V = 942.1(6)$ Å^3. Note that grinding feynmanite crystals

Table 6. Bond-valence analysis for feynmanite. Values are expressed in valence units.*

	O1	O2	O3	O4	O5	O6	OH	OW1	OW2	OW3	OW4a	OW4b	Sum
Na1					0.37 ×0.48↓	0.18 ×0.48↓		0.23 ×0.48↓		0.37 ×0.48↓	0.13	0.16	1.24
Na2	0.13 ×2→ ×0.60↓								0.13 ×0.60↓	0.10 ×2→ ×0.60↓	0.21 ×2→		1.01
Na3			0.07 ×0.19↓	0.08 ×0.19↓				0.38 ×0.19↓	0.36 ×0.38↓	0.32 ×0.19↓		0.10	1.31
U		0.46	0.48	0.47	1.81	1.79	0.54, 0.52						6.07
S	1.54	1.49	1.46	1.44									5.93
Sum	1.62	1.95	1.95	1.93	1.89	1.88	1.06	0.18	0.22	0.28	0.33	0.26	

*Multiplicity is indicated by ×↓→. The bond strength contributions from Na atoms to O atoms are factored by the occupancies of the Na sites, except for those to the partially occupied OW4a and OW4b sites. All bond-valence parameters are from Gagné and Hawthorne (2015). Hydrogen bonds are not included. Note that the low bond-valence sum for O1 may be compensated by a hydrogen bond from OH (OH···OW1 = 2.89 Å) or O1 may possess some OH character.

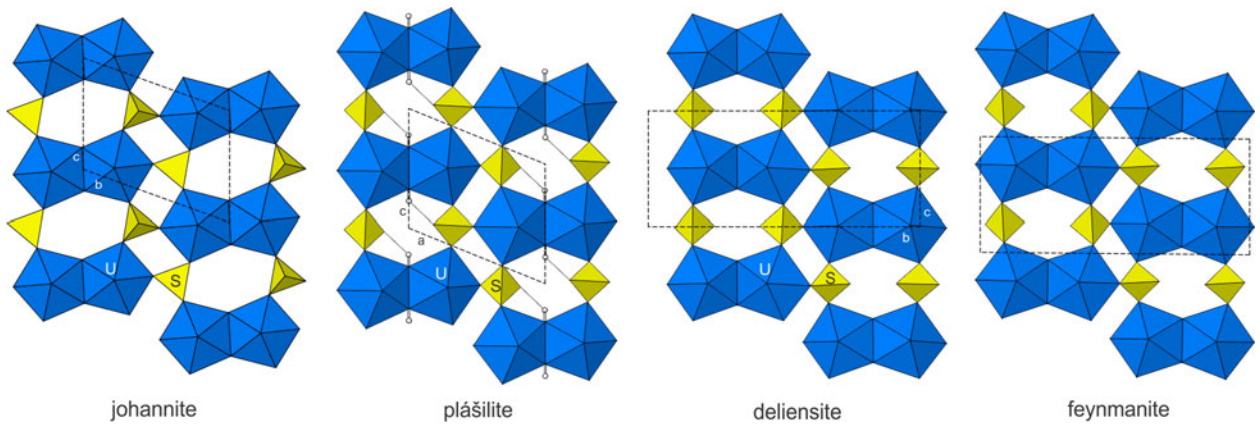

Fig. 5. Sheets in the structures of johannite, plášilite, deliensite and feynmanite. The unit cells are shown by dashed lines. For plášilite, H atoms are shown as white spheres and O–H bonds are shown as sticks. H atom positions were not determined in the other structures.

into a powder will promote its dehydration and is likely to yield a pattern more closely matching plášilite.

Single-crystal data were collected on a crystal from the Markey mine using MoKα X-rays from a microfocus source and an Apex II CCD-based detector mounted to a Bruker Apex II Quazar three-circle diffractometer. Reflections were integrated and corrected for Lorentz, polarisation and background effects using the Bruker program *SAINT*. A multi-scan semi-empirical absorption correction was applied using equivalent reflections in *SADABS-2012*. An initial structure model was obtained by the charge-flipping method using *SHELXT* (Sheldrick, 2015*a*) in the space group *P*2/*n*. Refinement proceeded by full-matrix least-squares on F^2 using *SHELXL-2016* (Sheldrick, 2015*b*). The structure solution located the U, S and seven O sites in the uranyl sulfate sheet (see below), as well as five sites between the sheets, initially identified as O sites. Based upon bonding geometry, two of the five interlayer sites were assigned as partially occupied Na atoms. A difference-Fourier synthesis located an additional partially occupied Na site and a split O site. All sites were successfully refined with anisotropic displacement parameters. A subsequent difference-Fourier synthesis failed to locate any likely H atom sites. The two highest electron density residuals, 3.76 and 3.67 e^- A^{-3}, were located within 1 Å of the U site. The next highest residual, 2.67 e^- A^{-3}, is located in the interlayer region 1.09 Å from Na1 and probably is related to the disorder; however, modelling it as an additional partially occupied site did not seem warranted. No other residuals >1.2 e^- A^{-3} are located in the interlayer region. Data collection and refinement details are given in Table 3, atom coordinates and displacement parameters in Table 4, selected bond distances in Table 5 and a bond-valence analysis in Table 6. The crystallographic information files have been deposited with the Principal Editor of *Mineralogical Magazine* and are available as Supplementary material (see below).

Description and discussion of the structure

The U site in the structure of feynmanite is surrounded by seven O atom sites forming a squat pentagonal bipyramid, which is a typical coordination for U^{6+} with the two short apical bonds of the bipyramid constituting the uranyl group. In the structure, pairs of pentagonal bipyramids share a common edge, forming dimers. The dimers are linked by sharing corners with SO_4 groups, yielding a $[(UO_2)_2(SO_4)_2(OH)_2]^{2-}$ sheet parallel to {010} (Fig. 5). Between the sheets are three fully occupied O sites and one split O site, all corresponding to H_2O groups. Also in the interlayer region are three partially occupied Na sites with a total occupancy corresponding to 0.97 apfu. Each Na site links to two O sites in the sheets; Na1 links to O sites in different sheets, while the Na2 and Na3 sites link to O sites in the same sheet. The Na1 and Na3 sites also each link to four interlayer O (H_2O) sites and the Na2 site also links to five interlayer O (H_2O) sites. The bonds between Na and O sites serve to link the sheets in the [010] direction (Fig. 6). Because of the complexity of the bonding in the interlayer region, the hydrogen bonding was not comprehensively analysed. The ideal structural formula is $Na(UO_2)(SO_4)(OH)\cdot 3.5H_2O$.

The $[(UO_2)_2(SO_4)_2(OH)_2]^{2-}$ sheet is based on the phosphuranylite anion topology (Burns, 2005), with a ring symbol $6^1 5^2 4^2 3^2$ (Krivovichev and Burns, 2007). The sheets in johannite, $Cu[(UO_2)_2(OH)_2(SO_4)_2]\cdot 8H_2O$ (Mereiter, 1982), deliensite, $Fe(UO_2)_2(SO_4)_2(OH)_2\cdot 7H_2O$ (Plášil *et al.*, 2012) and plášilite, $Na(UO_2)(SO_4)(OH)\cdot 2H_2O$ (Kampf *et al.*, 2015*b*), are topologically identical to that in feynmanite. The sheets in johannite and plášilite are geometrical isomers, differing in the orientation of the SO_4 groups, while that in deliensite is the same geometrical isomer as in feynmanite (Fig. 5).

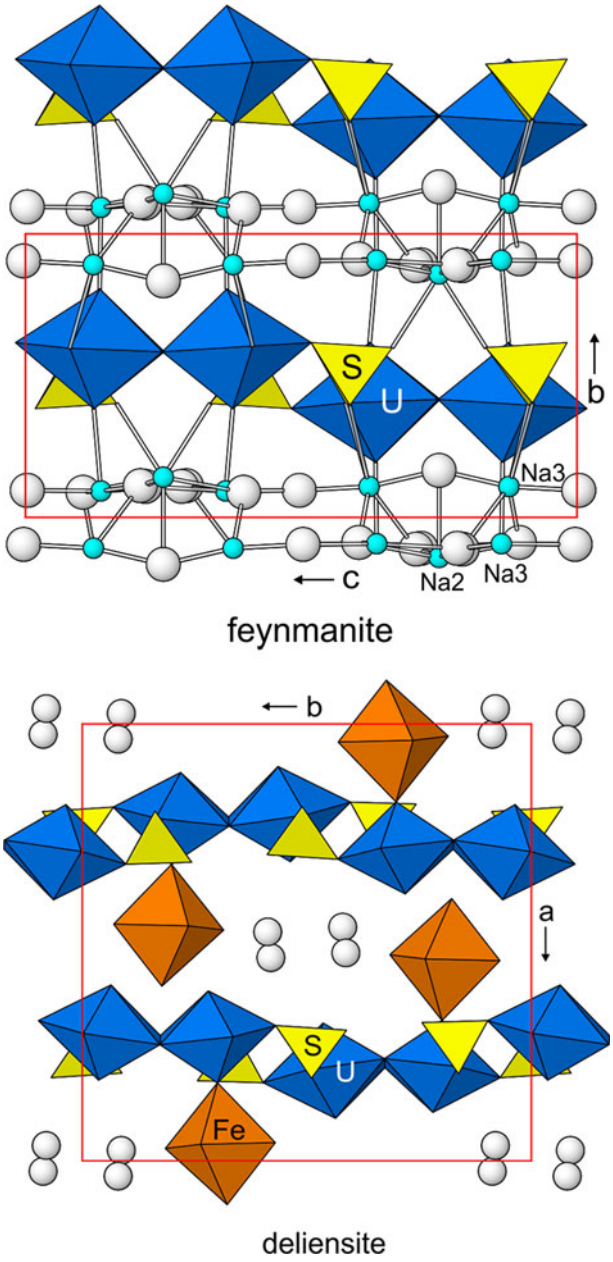

Fig. 6. The crystal structure of feynmanite compared with that of deliensite. The unit-cell outlines are in red. The O atoms of H_2O groups are shown as white spheres. Na–O bonds are drawn as sticks.

The formulas of feynmanite and plášilite differ only in their numbers of H_2O groups i.e. 3.5 H_2O pfu for feynmanite and 2 H_2O pfu for plášilite. Interestingly, the powder X-ray diffraction patterns of partially dehydrated feynmanite crystals exhibit lines apparently corresponding to both feynmanite and plášilite. It might be conjectured that the loss of H_2O from the interlayer region in the feynmanite structure results in reconfiguration into the plášilite structure; however, this would necessitate a reconfiguration of some of the SO_4 groups in the uranyl-sulfate sheet, which seems unlikely. Perhaps, a more likely possibility is

that the dehydration of feynmanite results in another phase that is very similar to plášilite structurally, but contains a $[(UO_2)_2(SO_4)_2(OH)_2]^{2-}$ sheet identical to that in feynmanite.

Finally, it should be noted that the structures of feynmanite and deliensite (Fig. 6), while they are based upon identical $[(UO_2)_2(SO_4)_2(OH)_2]^{2-}$ sheets (except for minor geometrical differences), have very different interlayer regions and, consequently, very different linkages between their sheets. The periodicity orthogonal to the sheets in the deliensite structure is double that in the feynmanite structure due to the relative lateral shifting between sheets in deliensite. Notably, in the deliensite structure, there are no O–cation–O linkages between the sheets, as the interlayer FeO_6 octahedra link only to one uranyl-sulfate sheet. Therefore, the sheets in deliensite are linked only by hydrogen bonding, while those in feynmanite are linked by a combination of O–Na1–O and hydrogen bonds.

Acknowledgements. Reviewer Fernando Cámara, Structures Editor Peter Leverett and Editorial Board Member Mark Welch are thanked for their constructive comments on the manuscript. A portion of this study was funded by the John Jago Trelawney Endowment to the Mineral Sciences Department of the Natural History Museum of Los Angeles County.

Supplementary material. To view supplementary material for this article, please visit https://doi.org/10.1180/mgm.2018.117

References

Bartlett J.R. and Cooney R.P. (1989) On the determination of uranium-oxygen bond lengths in dioxouranium(VI) compounds by Raman spectroscopy. *Journal of Molecular Structure*, **193**, 295–300.

Burns P.C. (2005) U^{6+} minerals and inorganic compounds: insights into an expanded structural hierarchy of crystal structures. *The Canadian Mineralogist*, **43**, 1839–1894.

Čejka J. (1999) Infrared spectroscopy and thermal analysis of the uranyl minerals. Pp. 521–622 in: *Uranium: Mineralogy, Geochemistry and the Environment* (P.C. Burns and R.C. Finch, editors). Reviews in Mineralogy, **38**. Mineralogical Society of America, Washington, DC.

Chenoweth W.L. (1993) The geology and production history of the uranium deposits in the White Canyon mining district, San Juan County, Utah. *Utah Geological Survey Miscellaneous Publication*, 93–3.

Gagné O.C. and Hawthorne F.C. (2015) Comprehensive derivation of bond-valence parameters for ion pairs involving oxygen. Acta Crystallographica, **B71**, 562–578.

Kampf A.R., Plášil J., Kasatkin A.V., Marty J. and Čejka J. (2015*a*) Fermiite, $Na_4(UO_2)(SO_4)_3$-$3H_2O$ and oppenheimerite, $Na_2(UO_2)(SO_4)_2{\cdot}3H_2O$, two new uranyl sulfate minerals from the Blue Lizard mine, San Juan County, Utah, USA. *Mineralogical Magazine*, **79**, 1123–1142.

Kampf A.R., Kasatkin A.V., Čejka J. and Marty J. (2015*b*) Plášilite, $Na(UO_2)(SO_4)(OH){\cdot}2H_2O$, a new uranyl sulfate mineral from the Blue Lizard mine, San Juan County, Utah, USA. *Journal of Geosciences*, **60**, 1–10.

Kampf A.R., Olds T.A., Plášil J., Marty J. and Perry S.N. (2017*a*) Feynmanite, IMA 2017-035. CNMNC Newsletter No. 38, August 2017, page 1037; *Mineralogical Magazine*, **81**, 1033–1038.

Kampf A.R., Plášil J., Kasatkin A.V., Marty J. and Čejka J. (2017*b*) Klaprothite, péligotite and ottohahnite, three new sodium uranyl sulfate minerals with bidentate UO_7–SO_4 linkages from the Blue Lizard mine, San Juan County, Utah, USA. *Mineralogical Magazine*, **81**, 753–779.

Kampf A.R., Plášil J., Kasatkin A.V., Marty J. and Čejka J. (2018) Markeyite, a new calcium uranyl tricarbonate mineral from the Markey mine, San Juan County, Utah, USA. *Mineralogical Magazine*, **81**, 1089–1100.

Krivovichev S.V. and Burns P.C. (2007) Actinide compounds containing hexavalent cations of the VI group elements (S, Se, Mo, Cr, W). Pp. 95–182 in: *Structural Chemistry of Inorganic Actinide Compounds* (S.V. Krivovichev, P.C. Burns and I.G. Tananaev, editors). Elsevier, Amsterdam.

Libowitzky E. (1999) Correlation of O-H stretching frequencies and O–H···O hydrogen bond lengths in minerals. *Monatshefte für Chemie*, **130**, 1047–1059.

Mandarino J.A. (1976) The Gladstone-Dale relationship – Part 1: derivation of new constants. *The Canadian Mineralogist*, **14**, 498–502.

Mandarino J.A. (2007) The Gladstone–Dale compatibility of minerals and its use in selecting mineral species for further study. *The Canadian Mineralogist*, **45**, 1307–1324.

Mereiter K. (1982) Die Kristallstrukturs des Johannits, $Cu(UO_2)_2(OH)_2(SO_4)_2{\cdot}8H_2O$. *Tschermaks Mineralogische und Petrographische Mitteilungen*, **30**, 47–57.

Plášil J., Buixaderas E., Čejka J., Sejkora J., Jehlička J. and Novák M. (2010) Raman spectroscopic study of the uranyl sulphate mineral zippeite: low wavenumber and U–O stretching regions. *Analytical and Bioanalytical Chemistry*, **397**, 2703–2715.

Plášil J., Hauser J., Petříček V., Meisser N., Mills S.J. , Škoda R., Fejfarová K., Čejka J., Sejkora J., Hloušek J., Johannet J.-M., Machovič V. and Lapčák L. (2012) Crystal structure and formula revision of deliensite, $Fe[(UO_2)_2(SO_4)_2(OH)_2](H_2O)_7$. *Mineralogical Magazine*, **76**, 2837–2860.

Pouchou J.L. and Pichoir F. (1985) "PAP" (φρZ) procedure for improved quantitative microanalysis. Pp. 104–106 in: *Microbeam Analysis* (J.T. Armstrong, editor). San Francisco Press, San Francisco, California, USA.

Sheldrick G.M. (2015*a*) SHELXT – Integrated space-group and crystal-structure determination. *Acta Crystallographica*, **A71**, 3–8.

Sheldrick G.M. (2015*b*) Crystal structure refinement with *SHELX*. *Acta Crystallographica*, **C71**, 3–8.

Volkovich V.A., Griffiths T.R., Fray D.J. and Fields M. (1998) Vibrational spectra of alkali metal (Li, Na and K) uranates and consequent assignment of uranate ion site symmetry. *Vibrational Spectroscopy*, **17**, 83–91.